JACS
JOURNAL OF THE AMERICAN CHEMICAL SOCIETY
Article
pubs.acs.org/JACS

Toward a Lithium–"Air" Battery: The Effect of CO_2 on the Chemistry of a Lithium–Oxygen Cell

Hyung-Kyu Lim,[†,§] Hee-Dae Lim,[‡,§] Kyu-Young Park,[‡] Dong-Hwa Seo,[∥] Hyeokjo Gwon,[⊥] Jihyun Hong,[‡] William A. Goddard, III,[†,#] Hyungjun Kim,[†,*] and Kisuk Kang[∥,*]

[†]Graduate School of Energy Environment Water Sustainability (EEWS), Korea Advanced Institute of Science and Technology (KAIST), 291 Daehak-ro, Yuseong-gu, Daejeon 305-701, Republic of Korea

[‡]Department of Materials Science and Engineering, Seoul National University, 1 Gwanak-ro, Gwanak-gu, Seoul 151-742, Republic of Korea

[∥]Center for Nanoparticle Research, Institute for Basic Science (IBS), and Department of Materials Science and Engineering, Research Institute of Advanced Materials, Seoul National University, 1 Gwanak-ro, Gwanak-gu, Seoul 151-742, Republic of Korea

[⊥]Department of Materials Science and Engineering, Korea Advanced Institute of Science and Technology (KAIST), 291 Daehak-ro, Yuseong-gu, Daejeon 305-701, Republic of Korea

[#]Materials and Process Simulation Center, Beckman Institute, California Institute of Technology, Pasadena, California 91125, United States

Supporting Information

ABSTRACT: Lithium–oxygen chemistry offers the highest energy density for a rechargeable system as a "lithium–air battery". Most studies of lithium–air batteries have focused on demonstrating battery operations in pure oxygen conditions; such a battery should technically be described as a "lithium–dioxygen battery". Consequently, the next step for the lithium–"air" battery is to understand how the reaction chemistry is affected by the constituents of ambient air. Among the components of air, CO_2 is of particular interest because of its high solubility in organic solvents and it can react actively with $O_2^{-\bullet}$, which is the key intermediate species in Li–O_2 battery reactions. In this work, we investigated the reaction mechanisms in the Li–O_2/CO_2 cell under various electrolyte conditions using quantum mechanical simulations combined with experimental verification. Our most important finding is that the subtle balance among various reaction pathways influencing the potential energy surfaces can be modified by the electrolyte solvation effect. Thus, a low dielectric electrolyte tends to primarily form Li_2O_2, while a high dielectric electrolyte is effective in electrochemically activating CO_2, yielding only Li_2CO_3. Most surprisingly, we further discovered that a high dielectric medium such as DMSO can result in the reversible reaction of Li_2CO_3 over multiple cycles. We believe that the current mechanistic understanding of the chemistry of CO_2 in a Li–air cell and the interplay of CO_2 with electrolyte solvation will provide an important guideline for developing Li–air batteries. Furthermore, the possibility for a rechargeable Li–O_2/CO_2 battery based on Li_2CO_3 may have merits in enhancing cyclability by minimizing side reactions.

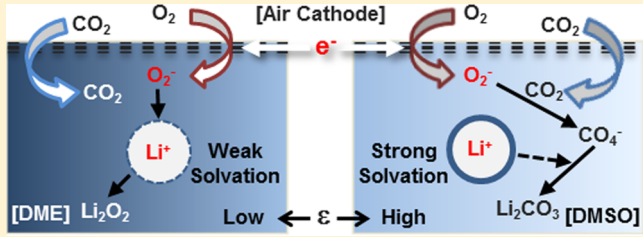

1. INTRODUCTION

The greatly increased demand for high energy density storage systems has heightened interest in Li–air batteries. A Li–air system potentially can deliver a gravimetric energy density of ~3500 Wh/kg (from the simple reaction of Li with dioxygen (O_2)), which is substantially higher than other battery types (e.g., ~600 Wh/kg for a $LiCoO_2$ system).[1−4] However, despite this great advantage in energy density,[5−7] major limitations in the reaction mechanism and its relation to the practical problems of Li–air batteries, which include poor cyclability, high polarization, and low rate capability, remain.[8−12] Furthermore, it is not yet known how the presence of the non-O_2 components of air affect the reaction mechanism in Li–air batteries because most previous studies have been conducted in a pure O_2 atmosphere, under the assumption that the other components of air will be less important in the operation of the battery.[13−16] To develop a Li–"air" battery technology usable at ambient conditions, it is critical to elucidate the effects of the other constituents of air (N_2, Ar, H_2O, and CO_2) on the operations of the Li–air battery.

Supposing that the moisture is removed by using water-proof films (which is known to fatally deteriorate electrolyte and lithium anode), CO_2 should have the most influence on the chemistry of the Li–air cell among the various constituents of air. Although N_2 and noble gases such as Ar are more abundant in ambient air, the conventional cathode voltage range of ~3 V cannot activate electrochemical reactions involving these gases and Li; for example, the theoretical formation potential is ~0.444 V for the reaction $3Li + {}^1/_2N_2 \rightarrow Li_3N$ [$\Delta_f G°(Li_3N) = -10.25$ kcal/mol/Li].[17] In contrast, CO_2 is known to be much less inert than N_2 or Ar, and it can therefore undergo electrochemical reactions with Li (some involving O_2 as well); for

Received: February 15, 2013
Published: June 11, 2013

   dx.doi.org/10.1021/ja4016765 | J. Am. Chem. Soc. 2013, 135, 9733−9742

example, the theoretical voltage for the formation of Li_2CO_3 is 3.82 V for the reaction $2Li + {}^1/_2O_2 + CO_2 \rightarrow Li_2CO_3$ [$\Delta_f G°(Li_2CO_3)$ = −135.30 kcal/mol/Li].[18] Additionally, Li_2CO_3 is a more chemically stable compound than Li_2O_2 [$\Delta_f G°(Li_2O_2)$ = −68.26 kcal/mol/Li].[18] The difference in chemical stability implies that there is always a thermodynamic driving force to convert Li_2O_2, the desired discharge product of a Li−air cell, into Li_2CO_3 in the presence of CO_2. This observation has also led people to believe that the irreversible formation of Li_2CO_3 might limit the cyclability of Li−"air" batteries.[19]

Moreover, the high solubility of CO_2 gas in organic electrolytes (~50 times more soluble than O_2)[20] results in the major possibility of CO_2 being incorporated in battery reactions, despite its low concentration in ambient air. Thus, to further the development of Li−air battery technology, it is critical to understand the reactions involving CO_2 and the chemistry of Li_2CO_3 within a Li−air cell. Although recent experimental studies have examined the effect of CO_2 gas in Li−air cells,[21,22] there remains no mechanistic understanding of how the Li−O_2 reaction pathways and Li−O_2/CO_2 reaction pathways will compete with each other and how the final discharge product will be regulated during electrochemical reactions in Li−air batteries.

In this work, we report both theoretical studies regarding the fundamental reaction mechanism and experimental studies of Li−air battery performance, which is significantly altered by the presence of CO_2. In particular, we showed that Li_2CO_3 can be selectively produced as a final discharge product depending on the dielectric properties of the electrolyte and demonstrated for the first time that Li_2CO_3 can undergo reversible reactions during the Li−O_2/CO_2 battery cycles

2. METHODS

Theoretical Calculation. We carried out quantum mechanical calculations based on density functional theory (DFT) using Jaguar 7.9.[23] We used the Becke three-parameter functional (B3)[24] combined with the correlation functional of Lee, Yang, and Parr (LYP),[25] along with the Pople 6-311++G** basis set.[26] The ground state geometries were fully optimized, and the transition state geometries were confirmed to have a single imaginary frequency. To describe various electrolytes,[27−30] solvation free energies were evaluated by using the PBF (Poisson−Boltzmann Finite element method),[31,32] as implemented in the Jaguar package. We used the experimental dielectric constant (ε) and calculated probe radii (R) from the molecular weight and liquid density of each electrolyte to describe the solvation of different electrolytes as listed in Table 1. The solvation energies of reactants, intermediates, and products were determined with self-consistently full optimizing solution phase geometries that include the atomic forces exerted by the implicit solvent in the reaction field. For the solvation energy of the transition state, we added the solvation energy calculated at the gas-phase transition state geometry in all cases, except the reaction of O_2^- with Li^+, as this gas-phase reaction is barrier-less. To evaluate the barrier energy for the reaction of O_2^- with Li^+, we calculated the solution phase reaction energy profile while changing the distance between O_2^- and Li^+ and then used the maximum value as the barrier energy (see Figure S2).

Table 1. Physical Properties of Selected Electrolytes

				solubility (mM)	
solvent	ε	probe radii, R (Å)	viscosity (cP)	O_2	CO_2
ethylene carbonate[47,48]	89.6	2.36	1.90	N/A	85.0
dimethyl sulfoxide[20]	47.2	2.41	1.95	2.1	125.0
dimethoxyethane[33]	7.2	2.77	0.46	9.6	N/A

*All properties are measured at 25 °C except for ethylene carbonate (40 °C).

Experimental Section. To evaluate reaction energies of oxidation/reduction, it is important to define the reference energy of the electron generated from the electrode. We defined this electron reference energy as the energy cost associated with dissolving a Li cation into the electrolyte from solid Li (see SI), which is the energy for the counter half-reaction occurring at the anode. This definition allows direct comparison of the reaction energy (ΔE) with the reduction potential values for a Li/Li^+ electrode (V) via the Nernst equation, $\Delta E \approx \Delta G = -nFV$ (where ΔG is the reaction free energy, F is the Faraday constant, and n is the number of electrons involved in the reactions). For example, the calculated reaction energies for the O_2 reduction reaction are 2.64 eV for dimethyl sulfoxide (DMSO) and 1.51 eV for dimethoxyethane (DME), which are reasonably close to the experimental values of ~2.3 (0.1 M $TBAPF_6$, DMSO) and ~1.8 V (0.1 M $TBAPF_6$, DME).[33]

The porous air electrode was composed of a mixture of Ketjen black carbon (EC 600JD, Ilshin Chemtech) and a binder (Kynal 2801) in a weight ratio of 8:2. *N*-Methyl-2-pyrrolidone (NMP, Sigma-Aldrich, 99.5%) was used as a dispersing agent. The mixtures were pasted onto a Ni mesh or carbon paper. The electrode was dried at 120 °C for 1 h to remove the residual NMP. Lithium metal ($^3/_8$ in. diameter), a glass fiber separator (Whatman GF/D microfiber filter paper, 2.7 μm pore size), and the air electrode were assembled into a Swagelok-type Li−air cell.[10] Either 0.21 mL of 1 M $LiPF_6$ in DMSO or 0.1 M $LiPF_6$ in DME was used as electrolyte. Each of the "Li−O_2 cells" was operated in a pure oxygen atmosphere at a pressure of 770 Torr, maintained at a constant value by using an automated throttle valve. The flow rate of gases was constantly maintained at 0.1 L/min and the total volume of gases for the one discharge is approximately 42−48 L. The "Li−O_2/CO_2 cells" were operated at a 1:1 pressure ratio of O_2 and CO_2, while all other conditions were identical with those for the Li−O_2 cells. The electrochemical properties were measured with a potentiogalvanostat (WonA Tech, WBCS 3000, Korea). The samples were characterized by using an X-ray diffractometer (XRD, D8-Advance, Bruker, Germany) equipped to measure Cu Kα radiation and the Fourier transform infrared (FTIR, FT-IR-4200, JASCO, Japan) spectra in an argon atmosphere. The morphologies of compounds were observed with use of a field emission scanning electron microscope (FE-SEM, Philips, XL 30 FEG, Eindhoven, Netherlands).

3. RESULTS AND DISCUSSION

QM Energetics at the Initial Complex Formation (ICF) Step. The sequential reactions occurring in the Li−O_2/CO_2 system were investigated by using DFT first-principles calculations. On the basis of the reduction potential of CO_2/CO_2^- (−2.0 V vs Ag in DMSO), which is about 1.6 V lower than that of O_2/O_2^- (−0.4 V vs Ag in DMSO),[20] it is reasonable to assume that the first reaction step is an "*oxygen reduction* reaction (ORR) step", as in a conventional Li−O_2 cell:[34,35]

$$O_2 + e^-(\text{electrode}) \rightarrow O_2^- \qquad (1.1)$$

After the oxygen molecule captures an electron from the cathode, a radical nucleophile reagent is created that can react vigorously with neutral or cationic species in the cell, such as CO_2, Li^+, or electrolytes. We designate this reaction step as the

dx.doi.org/10.1021/ja4016765 | J. Am. Chem. Soc. 2013, 135, 9733−9742

"*initial complex formation* (ICF) step" for the following discussion. This step consists of the following possible reactions:

$$O_2^- + Li^+ \rightarrow LiO_2 \quad (2.1)$$

$$O_2^- + CO_2 \rightarrow CO_4^- \quad (2.2)$$

$$O_2^- + \text{electrolyte} \rightarrow \text{decomposed electrolyte} \quad (2.3)$$

Figure 1 illustrates the possible reaction pathways for the ICF, including the reaction energy (ΔE) and the activation barrier ($\Delta E^{\ddagger}$) for this reaction in the three electrolyte-containing media (EC, DMSO, and DME). Detailed structural information for these chemical complexes is provided in the Supporting Information (Figure S1).

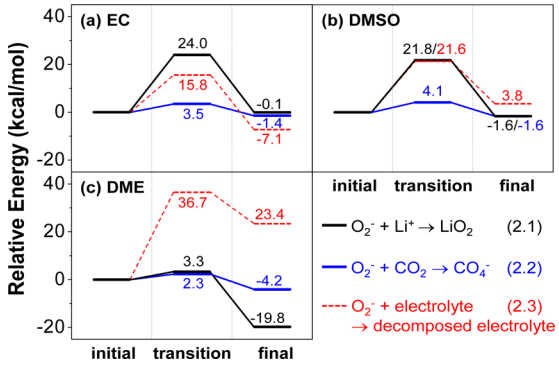

Figure 1. Activation barrier and binding reaction energy from DFT calculations at the initial complex formation (ICF) step, during which O_2^- is coordinating with Li^+ (black), CO_2 (blue), and electrolyte (red) with use of (a) EC (b) DMSO, and (c) DME electrolytes. To evaluate the activation barrier of the LiO_2 complex, which without solvation is a barrier-less downhill reaction, we scanned the reaction coordinate under an implicit solvation environment, with the maximum value determining the height of barrier (Figure S2).

In the electrolyte EC (Figure 1a), the reaction of the O_2^- radical with CO_2 is both thermodynamically and kinetically favored over its reaction with Li^+ (ΔE = −0.1 kcal/mol and $\Delta E^{\ddagger}$ = 24.0 kcal/mol for reaction 2.1; ΔE = −1.4 kcal/mol and $\Delta E^{\ddagger}$ = 3.5 kcal/mol for reaction 2.2). However, considering the possibility of O_2^- reacting also with surrounding electrolyte molecules reveals that a ring-opening reaction with EC (reaction 2.3) is the most thermodynamically favored, with ΔE = −7.1 kcal/mol (see Figure S1 for the structure of the decomposed EC). Thus, although the activation barrier ($\Delta E^{\ddagger}$) for reaction 2.3 (15.8 kcal/mol) is higher than that for reaction 2.2 (3.5 kcal/mol), the significantly higher stability of the final products of reaction 2.3 is expected to drive the reaction pathway toward decomposition of the EC electrolyte. This result is consistent with previous experiments with carbonate-based electrolytes in Li−O_2 cells[36] and explains why Li_2O_2 formation is not preferred in such systems. On the other hand, the electrolyte decomposition reaction 2.3 is not the most favored reaction in DMSO (Figure 1b) or in DME (Figure 1c) electrolytes. Here, the decomposition reaction is uphill (DMSO: 3.8 kcal/mol and DME: 23.4 kcal/mol), and the activation barriers are considerably higher than for reactions 2.1 and 2.2. This observation agrees well with recent findings that noncarbonate-based electrolytes are less susceptible to decomposition in Li−O_2 cells.[27,37−39]

Nevertheless, the reaction pathway for O_2^- in DMSO in the presence of CO_2 is clearly distinguishable from the corresponding reaction pathway in DME. Figure 1b shows that the reaction of O_2^- with Li^+ (reaction 2.1) results in a nearly identical energy state (ΔE = −1.6 kcal/mol) as does reaction with CO_2 (reaction 2.2) in DMSO. However, the activation barrier for reaction 2.1 is considerably higher than that for reaction 2.2, implying that the reaction of O_2^- with CO_2 is kinetically favored over its reaction with Li^+ in DMSO. In contrast, the reaction of O_2^- with Li^+ is much more likely in DME, as shown in Figure 1c. While the activation barriers for both reactions 2.1 and 2.2 in DME are comparable, the final state energy of reaction 2.1 is substantially more stable, indicating the dominant LiO_2 formation.

We attribute the clearly different behavior of the reactions of O_2^- during the ICF step in various electrolytes to the variation in the dielectric properties of the solvents. Generally, electrolytes with high dielectric constants (ε) effectively shield and thereby stabilize charged ionic species. To initiate such a reaction in a high dielectric electrolyte (such as EC or DMSO), the strongly coordinating solvent shell of a charged species such as Li^+ and O_2^- must be disrupted, at a considerable energy cost. Thus, reaction 2.1, which involves two individual charged species and their strongly coordinating solvent shells, requires a higher energy cost in EC (24.0 kcal/mol) and DMSO (21.8 kcal/mol) than is required in low dielectric DME (3.3 kcal/mol). In comparison, the reaction between O_2^- and CO_2 (reaction 2.2) is less sensitive to the dielectric behavior of electrolyte. Here, the reaction energies vary from −4.2 kcal/mol for DME to −1.4 kcal/mol for EC, with comparable activation energies. We attribute this to CO_2, a neutral species, not forming a strong solvation shell.

Figure 2 shows the DFT results for other organic solvents. We see correlation between the reaction energies for ICF (reactions 2.1 and 2.2) and the dielectric constant of the electrolyte. Here, it is noted that the reaction energies decrease linearly with the inverse of dielectric constant of electrolyte, particularly for reaction 2.1. However, the reaction of O_2^- with CO_2 (reaction 2.2) is affected by dielectric constant to a much lesser extent. The opposite behavior of these two reactions implies that for Li−O_2/CO_2 batteries, O_2^- is likely to react with

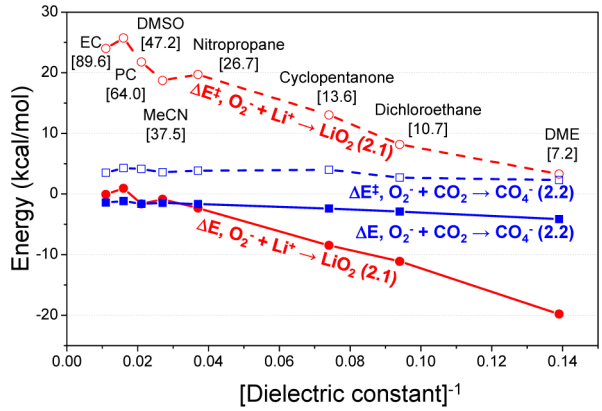

Figure 2. DFT predicted trend of activation barrier ($\Delta E^{\ddagger}$, dashed) and binding reaction energy (ΔE, solid) plotted against [dielectric constant]$^{-1}$ for the *initial complex formation* (ICF) steps of reactions 2.1 and 2.2, forming LiO_2 (red, circle) and CO_4^- (blue, square), respectively. The values enclosed in brackets are the dielectric constants of various solvents.

dx.doi.org/10.1021/ja4016765 | *J. Am. Chem. Soc.* 2013, 135, 9733−9742

CO_2 in a high dielectric solvent and more likely to react with Li^+ in a low dielectric solvent. Thus, at the ICF step, the reactions mostly depend on the dielectric constant. We recommend that these general dependencies of the chemistry on the dielectric constant be considered in choosing electrolytes for Li−air cells.

Reaction Pathways to the Final Products. In the following analysis, we focus only on the reaction pathways in DMSO and DME electrolytes because (i) carbonate electrolytes such as EC are susceptible to decomposition upon exposure to O_2^- and (ii) there have been complete studies published on this decomposition reaction.[28,39,40] In the subsequent DFT calculations, we examine the reaction pathways from the initial coordinated complexes, LiO_2 or CO_4^-, to monomeric Li_2O_2 and dimeric Li_2CO_3, which serve as the nuclei of the final discharge products. The initial LiO_2 complex can yield Li_2O_2 monomer via three possible pathways:

$$LiO_2 + Li^+ + e^-(\text{electrode}) \rightarrow Li_2O_2 \quad (3.1)$$

$$LiO_2 + Li^+ + O_2^- \rightarrow Li_2O_2 + O_2 \quad (3.2)$$

$$2LiO_2 \rightarrow Li_2O_2 + O_2 \quad (3.3)$$

Figure 3 compares the energetics of these three possible pathways in DMSO (Figure 3a) and DME (Figure 3b). We find

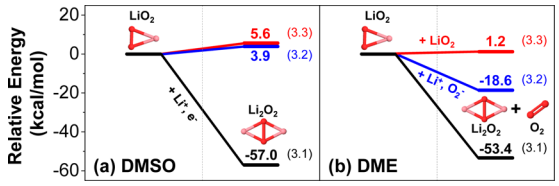

Figure 3. DFT relative energy changes from LiO_2 to Li_2O_2 for three possible reaction pathways with use of (a) DMSO and (b) DME electrolytes. Energies shown are for the direct reduction reaction (reaction 3.1) by electron transfer from electrode, for reduction by electron transfer from O_2^- (reaction 3.2), and for the dimerization of LiO_2 (reaction 3.3). The direct reduction reaction 3.1 is the most favored.

that reaction 3.1 is mostly favored over the other pathways regardless of the electrolyte (ΔE = −57.0 kcal/mol for DMSO and −53.4 kcal/mol for DME). Reaction 3.2 is a downhill process only in DME (not in DMSO), where ΔE = −18.6 kcal/mol for DME and 3.9 kcal/mol for DMSO. However, we note that the energy release of reaction 3.2, even in DME, is relatively small compared to that of reaction 3.1. On the other hand, formation of Li_2O_2 through the dimerization of LiO_2 (reaction 3.3) is endothermic in both electrolytes: 5.6 kcal/mol in DMSO and 1.2 kcal/mol in DME electrolyte. Therefore, Li_2O_2 monomer, a seed for the Li_2O_2 crystal, is expected to be formed via reaction 3.1, where the cathode reduces the LiO_2 complex while simultaneously capturing a Li^+ ion from the electrolyte. This result implies that once the initial complex LiO_2 is formed, Li_2O_2 can readily form in the vicinity of the electrode, which is consistent with the previous experimental study.[41]

The other possible discharge product in a Li−O_2/CO_2 cell is Li_2CO_3. Compared to Li_2O_2 formation, the reaction pathway for the formation of Li_2CO_3 is much more complicated because the initial complexes, Li^+, O_2^-, and CO_2, can undergo numerous possible intermediate reactions. Figure 4 illustrates the energetics for various reaction paths from O_2^- to Li_2CO_3 dimer in DMSO (Figure 4a) and DME (Figure 4b). The energies of all intermediate steps are calculated and shown as a colored map. For comparison, we also include the energy diagram for Li_2O_2 monomer formation along the *y*-axis. For simplicity, the reduction process during the incorporation of Li is depicted along the *y*-axis, while the corresponding process during CO_2 incorporation is depicted along the *x*-axis.

With regard to the incorporation of CO_2 (illustrated along the *x*-axis), we considered all reduction steps are conducted by electron transfer from O_2^- referring to the previous experiment.[42] Additionally, optimized structures of $C_2O_6^{3-}$ and $C_2O_6^{4-}$ with implicit solvation condition (produced by reduction of $C_2O_6^{2-}$, see Figure S3) indicate that the instability of the high charge concentration on this small molecule causes $C_2O_6^{2-}$ to dissociate breakage of the peroxide bridge between the two CO_3 molecules. This results in the dissociation of $C_2O_6^{2-}$ into CO_3^- and CO_3^{2-}, followed by further reduction of these species to two CO_3^{2-} molecules, as shown in the dotted box of Figure 4. However, we find another pathway suggesting that the reduction of $C_2O_6^{2-}$ via coordination with Li^+ ions is preferred to dissociation. The electrostatic attraction between $C_2O_6^{2-}$ and Li^+ dominates over the dissociation reaction for $C_2O_6^{2-}$, which requires the injection of an additional electron into the anion. This process yields a Li_2CO_3 dimer with a structure identical with the crystal unit of Li_2CO_3 (Figure S4).

We find that there are indeed multiple reaction pathways that result in the formation of Li_2CO_3 because the binding of Li^+ with most anionic intermediate species is exothermic. In this respect, it is reasonable to consider the steepest descending pathway on the energy landscape as the most probable pathway in the overall reaction mechanism. The most probable reaction pathways to form Li_2CO_3 from O_2^- are displayed with arrows in Figure 4 and tabulated in Tables 2 and 3. In the reaction to form Li_2CO_3, common pathways are generally shared in both DMSO and DME electrolytes. However, one notable difference in the most steeply descending pathways for each of the two electrolytes lies in the reduction of CO_4^-, as highlighted in Figure 4. In DMSO, the reduction of CO_4^- takes place with CO_2 incorporation in $C_2O_6^{2-}$, but in DME, this reduction involves Li^+ incorporation. We hypothesize that this dramatic difference arises from the difference in the dielectric behavior of two electrolytes. The high dielectric DMSO molecule allows stronger solvation of the charged species, thereby stabilizing the intermediate anion species. In contrast, the low dielectric DME molecule tends to neutralize the charged intermediates immediately due to weak solvation and charge screening. This trend is clearly observed throughout the overall reaction pathways.

Another important observation is that in the presence of CO_2, the final discharge products may differ between the DMSO and DME systems. In DMSO, because the Li_2O_2 formation pathway is kinetically blocked at the ICF step, as discussed above, Li_2CO_3 is expected to be the only discharge product. In DME, formation of both Li_2O_2 and Li_2CO_3 is kinetically and thermodynamically favored. However, considering that LiO_2 formation is heavily favored compared to CO_4^- formation at the ICF step, we anticipate Li_2O_2 to be a major discharge product in DME (but we note that the formation of Li_2CO_3 is unavoidable due to its thermodynamic stability, vide supra).

Experimental Validation in DMSO. To experimentally confirm the hypothesis that the dielectric property of the electrolyte influences the reaction pathway at the ICF step,

dx.doi.org/10.1021/ja4016765 | J. Am. Chem. Soc. 2013, 135, 9733−9742

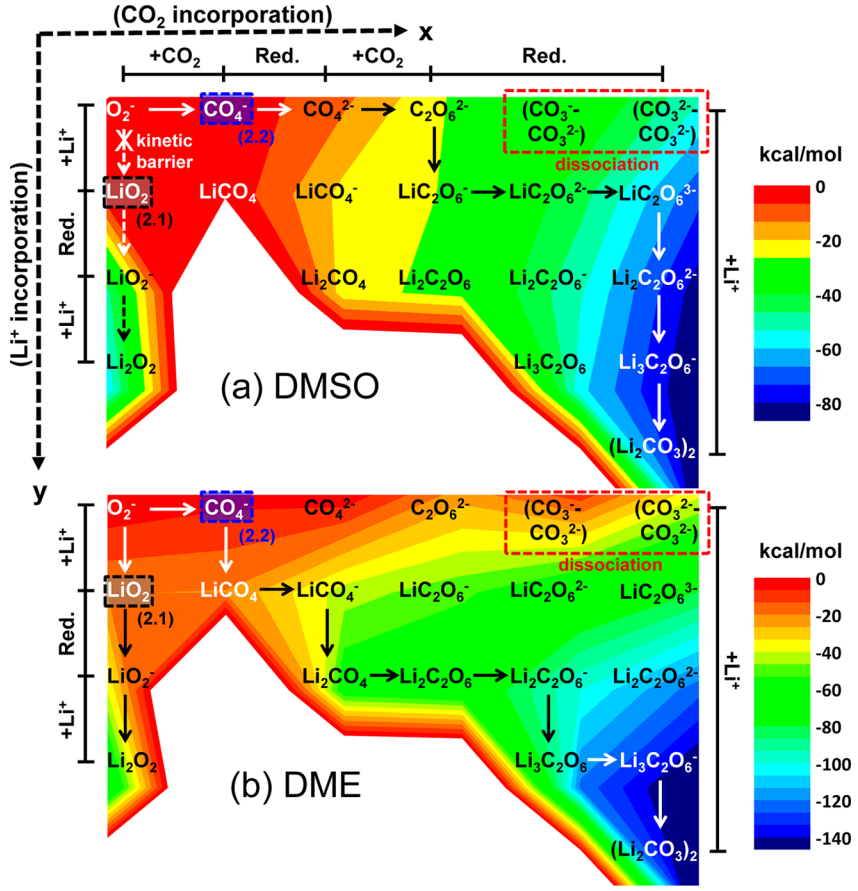

Figure 4. Two-dimensional energy surface map including every possible intermediate species from the dioxygen anion radical of O_2^- (formed after ORR reaction) to $(Li_2O_2)_1$ and $(Li_2CO_3)_2$ with use of DME and DMSO electrolytes. The most favorable reaction pathways to form the final products (the steepest descending pathways on the energy surface) are denoted with arrows and tabulated in Tables 2–4.

Table 2. Most Probable Reaction Pathway for Li_2CO_3 Formation with Use of DMSO Electrolyte, As Determined from DFT Calculations

elementary reaction	reaction energy (kcal/mol)
$4O_2 + 4e^-$ (electrode) $\rightarrow 4O_2^-$	-61.0×4
$O_2^- + CO_2 \rightarrow CO_4^-$	−1.6
$CO_4^- + O_2^- \rightarrow CO_4^{2-} + O_2$	−9.9
$CO_4^{2-} + CO_2 \rightarrow C_2O_6^{2-}$	−17.4
$C_2O_6^{2-} + Li^+ \rightarrow LiC_2O_6^-$	+0.9
$LiC_2O_6^- + O_2^- \rightarrow LiC_2O_6^{2-} + O_2$	−16.1
$LiC_2O_6^{2-} + O_2^- \rightarrow LiC_2O_6^{3-} + O_2$	−27.3
$LiC_2O_6^{3-} + Li^+ \rightarrow Li_2C_2O_6^{2-}$	−12.5
$Li_2C_2O_6^{2-} + Li^+ \rightarrow Li_3C_2O_6^-$	−4.1
$Li_3C_2O_6^- + Li^+ \rightarrow (Li_2CO_3)_2$	−6.3
$(Li_2CO_3)_2$ (soln) $\rightarrow (Li_2CO_3)_2$ (gas)	106.05
$(Li_2CO_3)_2$ (gas) $\rightarrow Li_2CO_3$ (cryst)	−119.42[a]
Overall: $O_2 + 2CO_2 + 4Li^+ + 4e^- \rightarrow (Li_2CO_3)_2$	**-351.22[b]**

[a]Calculated by using the periodic density functional theory method implemented in the Vienna Ab-initio Software Package (VASP) with PBE functional. [b]Using the Nernst equation, $\Delta E = -nFV$, the value can be converted into the reduction potential (V) of 3.81 V, where F is the Faraday constant and $n = 4$.

Table 3. Most Probable Reaction Pathway for Li_2CO_3 Formation with Use of DME Electrolyte, As Determined from DFT Calculations

elementary reaction	reaction energy (kcal/mol)
$4O_2 + 4e^-$ (electrode) $\rightarrow 4O_2^-$	-34.8×4
$O_2^- + CO_2 \rightarrow CO_4^-$	−4.2
$CO_4^- + Li^+ \rightarrow LiCO_4$	−16.3
$LiCO_4 + O_2^- \rightarrow LiCO_4^- + O_2$	−22.9
$LiCO_4^- + Li^+ \rightarrow Li_2CO_4$	−17.7
$Li_2CO_4 + CO_2 \rightarrow Li_2C_2O_6$	−7.4
$Li_2C_2O_6 + O_2^- \rightarrow Li_2C_2O_6^- + O_2$	−31.7
$Li_2C_2O_6^- + Li^+ \rightarrow Li_3C_2O_6$	−22.0
$Li_3C_2O_6 + O_2^- \rightarrow Li_3C_2O_6^- + O_2$	−31.9
$Li_3C_2O_6^- + Li^+ \rightarrow (Li_2CO_3)_2$	−25.0
$(Li_2CO_3)_2$ (soln) $\rightarrow (Li_2CO_3)_2$ (gas)	84.98
$(Li_2CO_3)_2$ (gas) $\rightarrow Li_2CO_3$ (cryst)	−119.42[a]
Overall: $O_2 + 2CO_2 + 4Li^+ + 4e^- \rightarrow (Li_2CO_3)_2$	**-352.74[b]**

[a]Calculated by using the periodic density functional theory method implemented in the Vienna Ab-initio Software Package (VASP) with PBE functional. [b]Using the Nernst equation, $\Delta E = -nFV$, the value can be converted into the reduction potential (V) of 3.82 V, where F is the Faraday constant and $n = 4$.

leading to different final discharge products in Li−O_2/CO_2 batteries, we constructed Li−air (O_2/CO_2) cell systems using both DMSO and DME as electrolytes. As a reference, we constructed a Li cell using pure O_2 and compared these results with the results from a Li−O_2/CO_2 cell. The operation of the reference Li−O_2 cell with use of DMSO in parts a and b of Figure 5 indicates that Li_2O_2 is the major discharge product, with trace amounts of LiOH, which is consistent with previous

dx.doi.org/10.1021/ja4016765 | J. Am. Chem. Soc. 2013, 135, 9733−9742

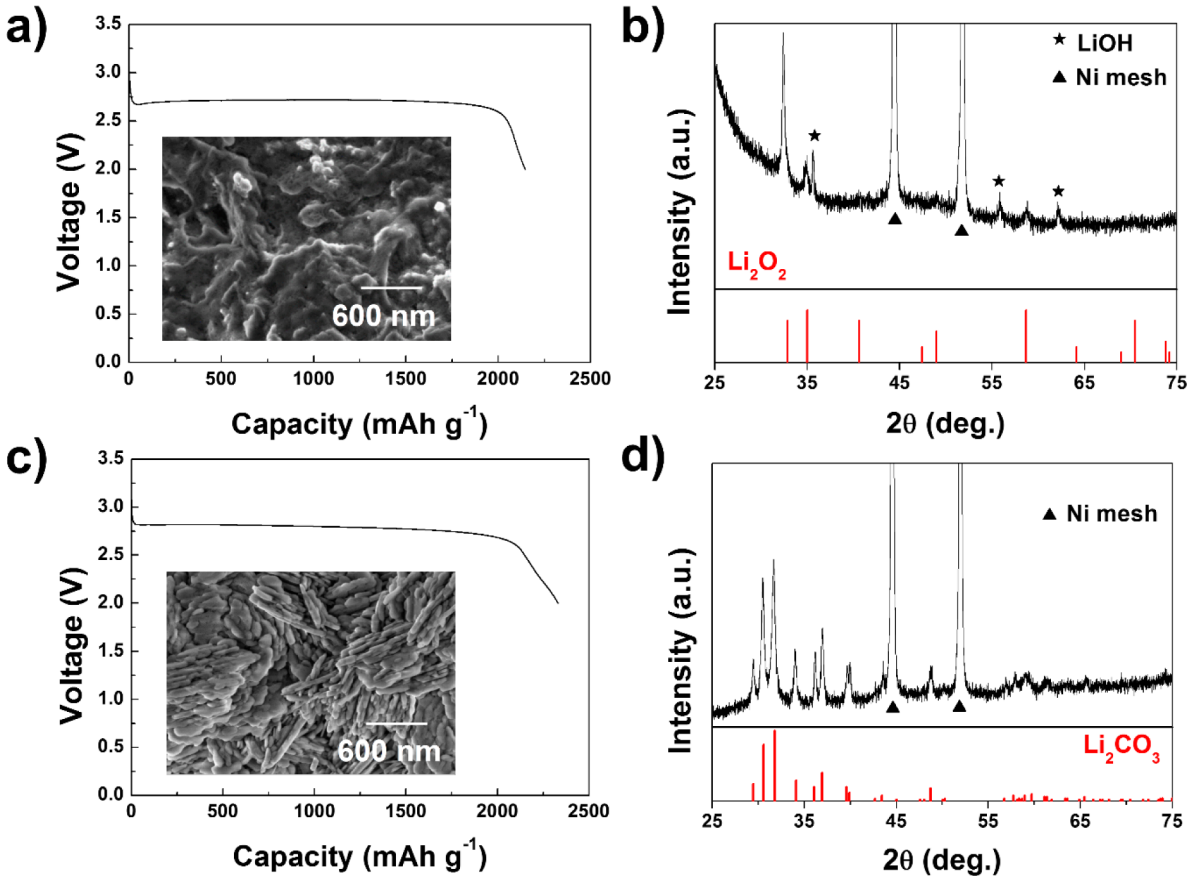

Figure 5. Electrochemical properties, SEM images, and XRD results of (a, b) a Li−O_2 cell and (c, d) a Li−O_2/CO_2 cell with DMSO electrolyte.

reports that some byproducts might be produced from the electrolyte decomposition or defective carbon surface.[27,30,49,50] However, a Li−O_2/CO_2 cell with the same DMSO electrolyte clearly shows different results, shown in parts c and d of Figure 5. While the discharge profile appears similar, with a comparable capacity of the reference cell, crystalline Li_2CO_3 is formed after the first discharge in the O_2/CO_2 mixed gas system. This stands in striking contrast to the conventional Li−O_2 cells, which produce Li_2O_2 as a major discharge product as well as trace amounts of Li_2CO_3 resulting from the degradation of the electrolyte and/or carbon cathode surface. Since Li_2CO_3 derived from the defective carbon or the electrolyte decomposition is usually amorphous and nondetectable from XRD patterns, the observed high crystallinity of Li_2CO_3 convinces that CO_2 gas is incorporated in the electrochemical reactions of the O_2/CO_2 mixed gas system to yield Li_2CO_3. Moreover, we find that the morphology of the discharge product in the Li−O_2/CO_2 cell is clearly different from that in the Li−O_2 cell. The discharge products in the Li−O_2/CO_2 cell grow in a flake-like shape with a preferred orientation, as shown in the inset of Figure 5c; however, the Li−O_2 cell (as shown in the inset of Figure 5a) produces discharge products without a particular shape, consistent with previous reports.[23,27,37] It should also be noted that the discharge potential is slightly higher (by 0.1 V) in the Li−O_2/CO_2 cell; this will be discussed in further detail later in this paper.

GITT measurements also indicate that the reaction mechanism and final products are different in the presence of CO_2. As shown in Figure 6, after a full relaxation of the potential (dV/dt: ~3.38 × 10^{-6} V s^{-1}), the equilibrium

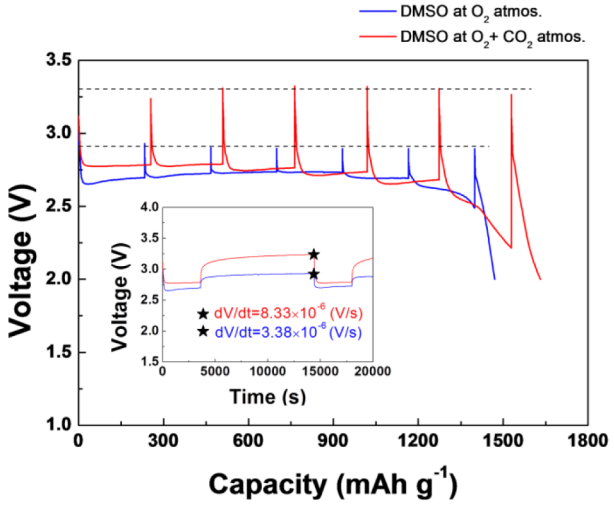

Figure 6. GITT discharge voltage profile obtained for a Li−O_2 cell (blue) and a Li−O_2/CO_2 cell (red) with DMSO electrolyte (inset: the potential vs time plot). The inset shows that the relaxation time is sufficient for each cell.

potential of the Li−O_2 cell (blue) reaches a value near 2.9 V regardless of the state of charge (SOC). This value compares well with the DFT formation potential of the major discharge product, Li_2O_2, which is 2.96 V.[1,43] In contrast, identical GITT measurements on the Li−O_2/CO_2 cell (red) show that the equilibrium potential is substantially higher, ~3.3 V. While comparing the open-circuit voltage does not provide direct evidence for Li_2CO_3 formation, it is noteworthy that the

dx.doi.org/10.1021/ja4016765 | J. Am. Chem. Soc. 2013, 135, 9733−9742

formation potential of Li_2CO_3 is 3.82 V, which is higher than that of Li_2O_2. These values are comparable to our DFT results for the calculated formation potentials of 2.90 V to yield Li_2O_2 and 3.81 V to yield Li_2CO_3, respectively (refer to the footnotes of Tables 2 and 4).

Table 4. Most Probable Reaction Pathway for Li_2O_2 Formation with Use of DMSO and DME Electrolytes

	reaction energy (kcal/mol)	
elementary reaction	DMSO	DME
$O_2 + e^- \text{ (electrode)} \rightarrow O_2^-$	−61.0	−34.8
$O_2^- + Li^+ \rightarrow LiO_2$	−1.6	−19.8
$LiO_2 + e^- \text{ (electrode)} \rightarrow LiO_2^-$	−47.4	−19.7
$LiO_2^- + Li^+ \rightarrow (Li_2O_2)_1$	−9.7	−33.7
$(Li_2O_2)_1$ (soln) $\rightarrow (Li_2O_2)_1$ (gas)	64.46	51.81
$(Li_2O_2)_1$ (gas) $\rightarrow Li_2O_2$ (cryst)[a]	−78.57	−78.57
Overall: $O_2 + 2Li^+ + 2e^- \rightarrow (Li_2O_2)_1$	**-133.804**[b]	**-134.755**[c]

[a]Calculated by using the periodic density functional theory method implemented in the Vienna Ab-initio Software Package (VASP) with PBE functional. [b]Using the Nernst equation, $\Delta E = -nFV$, the value can be converted into the reduction potential (V) of 2.90 V, where F is the Faraday constant and $n = 2$. [c]Using the Nernst equation, $\Delta E = -nFV$, the value can be converted into the reduction potential (V) of 2.92 V, where F is the Faraday constant and $n = 2$.

Experimental Validation in DME. Identical experiments on Li−O_2 and Li−O_2/CO_2 cells were performed in the DME electrolyte. For the reference Li−O_2 cell with DME, parts a and b of Figure 7 clearly show the formation of crystalline Li_2O_2 after the discharge process, in agreement with previous experimental reports.[28,44] However, for the Li−O_2/CO_2 cell, we found that the discharge process deposits an amorphous product. XRD could not identify the phase of this product, but FT-IR revealed that the discharge product was a mixture of Li_2O_2 and Li_2CO_3 (the inset of Figure 7d). Despite the similar intensity of the IR peaks for Li_2O_2 and Li_2CO_3, we cannot conclude that the quantities of both products present are comparable to each other because IR data are largely dependent on the composition of the surface, and Li_2O_2 can readily absorb CO_2 under CO_2-rich conditions, resulting in partial conversion of Li_2O_2 into Li_2CO_3 at the surface region.

Although there is no obvious way to characterize the major final discharge product when DME electrolyte is used, we can obtain some valuable information regarding the major products by examining the difference in discharge capacities presented in parts a and c of Figure 7, which show that the discharge capacity of the Li−O_2/CO_2 cell is half that of the Li−O_2 cell. Assuming that the activities of O_2 and CO_2 are comparable, the discharge capacity of the Li−O_2 and the Li−O_2/CO_2 cells should be similar, even though the discharge products are different (Li_2O_2 vs Li_2CO_3). However, given that the partial pressure ratio of O_2 and CO_2 is 1:1, our observation that the capacity of the Li−O_2/CO_2 cell is reduced by half allows us to deduce that CO_2 is significantly less electrochemically active compared to O_2. Thus, primarily Li_2O_2 is formed during the discharge process. In additional experiments with different ratios of O_2 and CO_2 (Figure S5), we confirmed that the overall discharge capacity is proportional to the partial pressure of oxygen in DME.[33,34] In contrast, in the case of DMSO, discharge capacity remains essentially constant regardless of the oxygen partial pressure because CO_2 is electrochemically active,

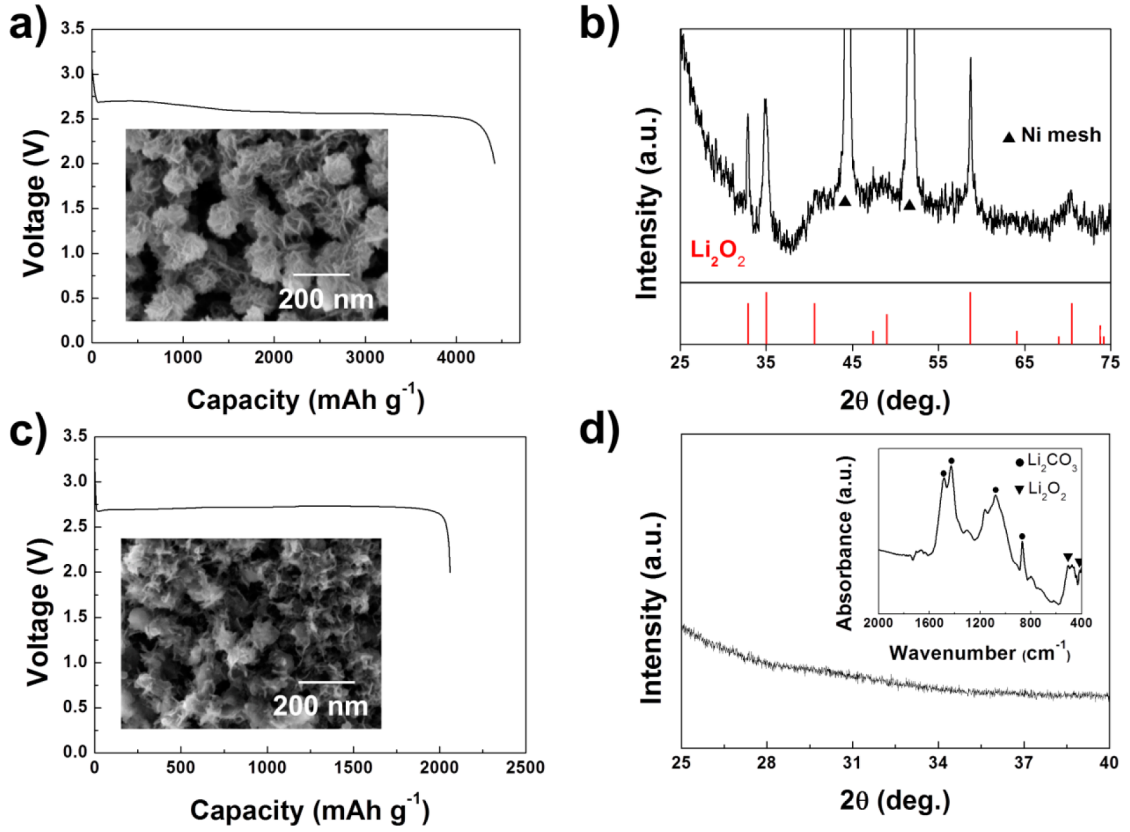

Figure 7. Electrochemical properties, SEM images, and XRD results of (a, b) a Li−O_2 cell and (c, d) a Li−O_2/CO_2 cell with DME electrolyte.

dx.doi.org/10.1021/ja4016765 | J. Am. Chem. Soc. 2013, 135, 9733−9742

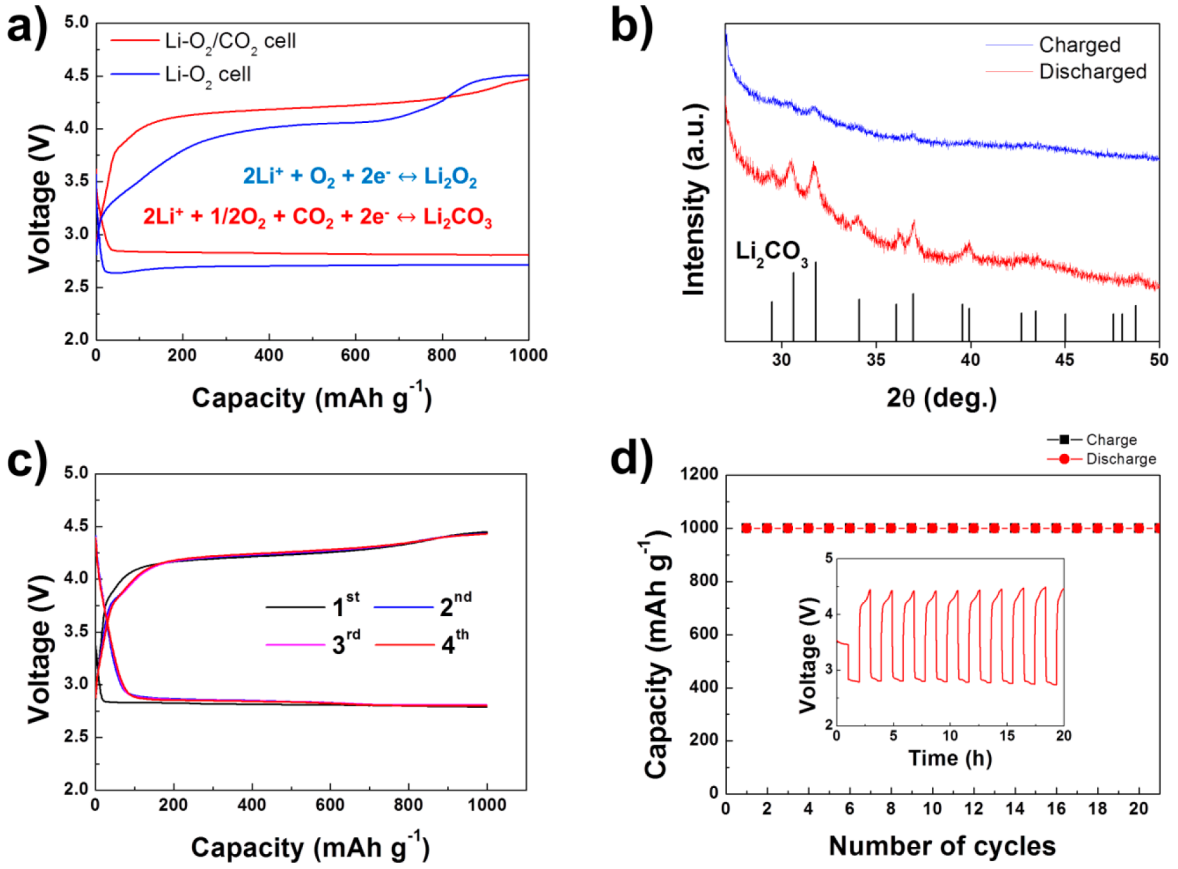

Figure 8. (a) The first discharge/charge profiles in each system with DMSO electrolyte, (b) XRD patterns after discharge and charge of the Li−O_2/CO_2 cell with DMSO electrolyte, (c) the initial 4 cycle profiles, and (d) the related cyclability of the Li−O_2/CO_2 cell, utilized up to 1000 mAh g^{-1} at a constant rate of 0.4 mA cm^{-2}.

and therefore, contributes equally to the capacity. Thus, it is quite reasonable to consider Li_2O_2 as the major initial discharge product in DME, which is in excellent agreement with our DFT predictions.

Even though the particle morphology does not provide direct evidence of particular phases, the growth behavior can provide additional information regarding the phase identity. As shown in the insets of Figure 7a,c, the morphologies of the discharge products in DME are macroscopically similar. This is in clear contrast with the case of DMSO, where the morphologies of the discharge products were notably different between the Li−O_2 cell and the Li−O_2/CO_2 cell. The similar morphological characteristic of discharge products was attributed to the comparable discharge processes of Li−O_2 and Li−O_2/CO_2 cells in DME.

Rechargeability of the Li−O_2/CO_2 Cell. As previously mentioned, based on the relative formation energies of Li_2O_2 and Li_2CO_3 and as demonstrated by using our Li−O_2/CO_2 cells with DME, the partial formation of Li_2CO_3 is inevitable in the presence of CO_2. Consequently, for the development of secondary Li−air batteries, it is important to preserve the electrochemical decomposability of Li_2CO_3. Thus, we further investigated the possibility of a rechargeable Li−O_2/CO_2 battery using DMSO as an electrolyte, based on the reversible formation and decomposition of Li_2CO_3.

As shown in Figure 8a, the first discharge/charge profile of the Li−O_2/CO_2 cell is notably different from that of the conventional Li−O_2 cell. The operating potential of the Li−O_2/CO_2 cell (red) is slightly higher than that of the conventional Li−O_2 cell (blue), which we attribute to the greater formation energy of Li_2CO_3 compared to Li_2O_2. The three steps observed in the charge profile of the Li−O_2 cell are consistent with previous results, based on the decomposition of Li_2O_2.[28,37,38] We note that the flat charge potential observed experimentally near 4.2 V in the Li−O_2/CO_2 cell corresponds to the potential for Li_2CO_3 decomposition in a Li−O_2 cell using a carbonate-based electrolyte.[28,39] The distinguishable electrochemical profiles of both cells again provide support for the differing reaction chemistry in Li−air cells depending on the constituents of the gas.

The XRD analysis of the Li−O_2/CO_2 cell, presented in Figure 8b, demonstrates that the discharge product, Li_2CO_3, is decomposed reversibly by an electrochemical oxidation process under 4.5 V. Although a trace amount of Li_2CO_3 exists after the charge, it certainly demonstrates that the high dielectric medium of DMSO can be effective in electrochemically activating CO_2. This suggests that a rechargeable battery based on Li_2CO_3 chemistry is feasible. At this point, we note that production of Li_2CO_3 has resulted from the input of CO_2 into the Li−air cell, not from the decomposition of electrolyte that is commonly observed in Li−air cells that use carbonate-based electrolytes.[15,29]

The rechargeability of the Li−O_2/CO_2 cell, based on the chemistry of Li_2CO_3, was further tested, as shown in Figure 8c,d. The cells were operated with capacity-limited cycling, which is presently often used to investigate the cyclability of Li−air batteries.[13,45,46] Quite interestingly, prolonged cycles without any catalysts or additives show a stable reversible

dx.doi.org/10.1021/ja4016765 | J. Am. Chem. Soc. 2013, 135, 9733−9742

reaction. We note that this is an outstanding result compared to previous reports based on Li−O_2 cells with carbonate-type electrolytes (where serious electrolyte decomposition deteriorates the cell cyclability) or even compared with the Li−O_2 cell with DMSO electrolyte (where byproducts, such as LiOH, can be produced continuously over many cycles[27,30]). Indeed, our analysis of the final product shows that there is only a single discharge product, Li_2CO_3, without any other byproducts, such as LiOH. We expect that the outstanding thermodynamic stability of Li_2CO_3 minimizes the possibility of side reactions, leading to the enhanced cyclability of these systems. This also suggests that reaction design to inhibit the formation of LiOH should be the next advance made in the development of practical Li−air batteries.

4. CONCLUSION

To further progress toward their practical application, Li−air batteries must be operated in an ambient air environment consisting of O_2, CO_2, N_2, etc. Thus, in this study, we investigated the effect of CO_2, the gas component of ambient air that most influences the chemistry of Li−air cells. On the basis of quantum mechanical (QM) calculations coupled with experiments, we described the reaction chemistry of a Li−"air" cell consisting of Li, O_2, and CO_2 during the initial stage of battery operation. We found that the electrolyte solvation effect can be useful for leveraging the reaction pathway at the *initial complex formation* (ICF) step by altering the potential energy surface, which is predicted to change the final discharge product of the Li−air cell. Indeed, our experimental results from a Li−O_2/CO_2 cell showed that the high dielectric DMSO favors electrochemical activation of CO_2 to form Li_2CO_3, while the low dielectric DME tends to form Li_2O_2 as a major discharge product, consistent with the theoretical investigations.

Furthermore, we determined, for the first time, that the electrochemical activation of CO_2 within the high dielectric medium of DMSO enables the reversible formation of Li_2CO_3 instead of Li_2O_2. This is of vital importance because the superior thermodynamic stability of Li_2CO_3 leads to its formation being unavoidable in an environment containing CO_2. Moreover, the realization of cell cycling based on the stability of Li_2CO_3 seems to help attain a more stable cyclability for Li−air cells.

On the basis of our systematic investigation of the reaction chemistry of CO_2 within a Li−air battery cell combined with the idea of "reaction pathway leveraging using dielectric media", we suggest that the use of a high dielectric electrolyte may help to preserve the reversible reaction of Li_2CO_3 by electrochemically activating CO_2. However, we should note that the electrolytes with the highest dielectric constants are usually either protic or carbonate-type; the former is not suitable for Li−ion chemistry and the latter has stability problems. Thus, DMSO might be optimal. In addition, our findings might further open up the new possibility for a novel rechargeable Li−O_2/CO_2 battery based on the single discharge product of Li_2CO_3, which has proven advantageous with regard to cyclability.

■ ASSOCIATED CONTENT

Supporting Information

Detail information of computational calculations, electrochemical properties, and XRD results of Li−O_2/CO_2 cells at a 9:1 pressure ratio of O_2 and CO_2. This material is available free of charge via the Internet at http://pubs.acs.org.

■ AUTHOR INFORMATION

Corresponding Author

matlgen1@snu.ac.kr; linus16@kaist.ac.kr

Author Contributions

[§]These authors contributed equally.

Notes

The authors declare no competing financial interest.

■ ACKNOWLEDGMENTS

This work was supported by the National Research Foundation of Korea Grant funded by the Korean Government (MEST) (NRF-2009-0094219) and supported by Human Resources Development of the Korea Institute of Energy Technology Evaluation and Planning (KETEP) grant funded by the Korea government Ministry of Knowledge Economy (20114010203120). This work was also supported by the Industrial Strategic Technology Development Program (No. 10038617, Development of Next Generation Lithium Metal Battery for the Full EVs) funded by the Ministry of Knowledge Economy (MKE, KOREA). H.-K.L., W.A.G., and H.K. are thankful for financial support by the National Research Foundation of Korea (NRF) grant funded by the Ministry of Education, Science and Technology (MEST) (2012M1A2A2026588) and the World Class University program (R-31-2008-000-10055-0).

■ REFERENCES

(1) Bruce, P. G.; Freunberger, S. A.; Hardwick, L. J.; Tarascon, J.-M. *Nat. Mater.* **2012**, *11*, 19.

(2) Leskes, M.; Drewett, N. E.; Hardwick, L. J.; Bruce, P. G.; Goward, G. R.; Grey, C. P. *Angew. Chem.* **2012**, *124*, 8688.

(3) Black, R.; Oh, S. H.; Lee, J.-H.; Yim, T.; Adams, B.; Nazar, L. F. *J. Am. Chem. Soc.* **2012**, *134*, 2902.

(4) Hartmann, P.; Bender, C. L.; Vračar, M.; Dürr, A. K.; Garsuch, A.; Janek, J.; Adelhelm, P. *Nat. Mater.* **2012**, *12*, 228.

(5) Li, Y.; Wang, J.; Li, X.; Liu, J.; Geng, D.; Yang, J.; Li, R.; Sun, X. *Electrochem. Commun.* **2011**, *13*, 668.

(6) Wang, Z.-L.; Xu, D.; Xu, J.-J.; Zhang, L.-L.; Zhang, X.-B. *Adv. Funct. Mater.* **2012**, *22*, 3699.

(7) Oh, S. H.; Nazar, L. F. *Adv. Energy Mater.* **2012**, *2*, 903.

(8) Freunberger, S. A.; Chen, Y.; Drewett, N. E.; Hardwick, L. J.; Bardé, F.; Bruce, P. G. *Angew. Chem.* **2011**, *50*, 8609.

(9) Débart, A.; Paterson, A. J.; Bao, J.; Bruce, P. G. *Angew. Chem.* **2008**, *120*, 4597.

(10) Lim, H.-D.; Park, K.-Y.; Song, H.; Jang, E. Y.; Gwon, H.; Kim, J.; Kim, Y. H.; Lima, M. D.; Robles, R. O.; Lepró, X.; Baughman, R. H.; Kang, K. *Adv. Mater.* **2012**, *25*, 1348.

(11) Shui, J.-L.; Karan, N. K.; Balasubramanian, M.; Li, S.-Y.; Liu, D.-J. *J. Am. Chem. Soc.* **2012**, *134*, 16654.

(12) Jung, K.-N.; Lee, J.-I.; Im, W. B.; Yoon, S.; Shin, K.-H.; Lee, J.-W. *Chem. Commun.* **2012**, *48*, 9406.

(13) Lim, H.-D.; Park, K.-Y.; Gwon, H.; Hong, J.; Kim, H.; Kang, K. *Chem. Commun.* **2012**, *48*, 8374.

(14) Lin, X.; Zhou, L.; Huang, T.; Yu, A. *J. Mater. Chem. A* **2013**, *1*, 1239.

(15) Li, Y.; Wang, J.; Li, X.; Geng, D.; Banis, M. N.; Tang, Y.; Wang, D.; Li, R.; Sham, T.-K.; Sun, X. *J. Mater. Chem.* **2012**, *22*, 20170.

(16) Cui, Y.; Wen, Z.; Liang, X.; Lu, Y.; Jin, J.; Wu, M.; Wu, X. *Energy Environ. Sci.* **2012**, *5*, 7893.

(17) Nam, S. C.; Yoon, Y. S.; Cho, W. I.; Cho, B. W.; Chun, H. S.; Yun, K. S. *J. Electrochem. Soc.* **2001**, *148*, A220.

(18) Dean, J. A. In *Lange's Handbook of Chemistry*, 12th ed.; McGraw-Hill: New York, NY, 1979; Vol. 9, p 4.

(19) Christensen, J.; Albertus, P.; Sanchez-Carrera, R. S.; Lohmann, T.; Kozinsky, B.; Liedtke, R.; Ahmed, J.; Kojic, A. *J. Electrochem. Soc.* **2012**, *159*, R1.
(20) Wadhawan, J. D.; Welford, P. J.; Maisonhaute, E.; Climent, V.; Lawrence, N. S.; Compton, R. G.; McPeak, H. B.; Hahn, C. E. W. *J. Phys. Chem. B* **2001**, *105*, 10659.
(21) Takechi, K.; Shiga, T.; Asaoka, T. *Chem. Commun.* **2011**, *47*, 3463.
(22) Gowda, S. R.; Brunet, A.; Wallraff, G. M.; McCloskey, B. D. *J. Phys. Chem. Lett.* **2012**, 276.
(23) Suite 2012: Jaguar version 7.9, S., LLC, New York, NY, 2012.
(24) Becke, A. D. *J. Phys. Chem.* **1993**, *98*, 5648.
(25) Lee, C. T.; Yang, W. T.; Parr, R. G. *Phys. Rev. B* **1988**, *37*, 785.
(26) Harihara, P.; Pople, J. A. *Chem. Phys. Lett.* **1972**, *16*, 217.
(27) Xu, D.; Wang, Z.-l.; Xu, J.-j.; Zhang, L.-l.; Zhang, X.-b. *Chem. Commun.* **2012**, *48*, 6948.
(28) McCloskey, B. D.; Bethune, D. S.; Shelby, R. M.; Girishkumar, G.; Luntz, A. C. *J. Phys. Chem. Lett.* **2011**, *2*, 1161.
(29) Wang, H.; Xie, K. *Electrochim. Acta* **2012**, *64*, 29.
(30) Xu, D.; Wang, Z.-L.; Xu, J.-J.; Zhang, L.-L.; Wang, L.-M.; Zhang, X.-B. *Chem. Commun.* **2012**, *48*, 11674.
(31) Tannor, D. J.; Marten, B.; Murphy, R.; Friesner, R. A.; Sitkoff, D.; Nicholls, A.; Ringnalda, M.; Goddard, W. A.; Honig, B. *J. Am. Chem. Soc.* **1994**, *116*, 11875.
(32) Marten, B.; Kim, K.; Cortis, C.; Friesner, R. A.; Murphy, R. B.; Ringnalda, M. N.; Sitkoff, D.; Honig, B. *J. Phys. Chem.* **1996**, *100*, 11775.
(33) Laoire, C. O.; Mukerjee, S.; Abraham, K. M.; Plichta, E. J.; Hendrickson, M. A. *J. Phys. Chem. C* **2010**, *114*, 9178.
(34) Hassoun, J.; Croce, F.; Armand, M.; Scrosati, B. *Angew. Chem.* **2011**, *50*, 2999.
(35) Hassoun, J.; Jung, H.-G.; Lee, D.-J.; Park, J.-B.; Amine, K.; Sun, Y.-K.; Scrosati, B. *Nano Lett.* **2012**, *12*, 5775.
(36) Bryantsev, V. S.; Giordani, V.; Walker, W.; Blanco, M.; Zecevic, S.; Sasaki, K.; Uddin, J.; Addison, D.; Chase, G. V. *J. Phys. Chem. A* **2011**, *115*, 12399.
(37) Xu, D.; Wang, Z.-l.; Xu, J.-j.; Zhang, L.-l.; Wang, L.-m.; Zhang, X.-b. *Chem. Commun.* **2012**, *48*, 11674.
(38) Laoire, C.; Mukerjee, S.; Plichta, E. J.; Hendrickson, M. A.; Abraham, K. M. *J. Electrochem. Soc.* **2011**, *158*, A302.
(39) Freunberger, S. A.; Chen, Y.; Peng, Z.; Griffin, J. M.; Hardwick, L. J.; Bardé, F.; Novák, P.; Bruce, P. G. *J. Am. Chem. Soc.* **2011**, *133*, 8040.
(40) Zhang, Z.; Lu, J.; Assary, R. S.; Du, P.; Wang, H. H.; Sun, Y. K.; Qin, Y.; Lau, K. C.; Greeley, J.; Redfern, P. C.; Iddir, H.; Curtiss, L. A.; Amine, K. *J. Phys. Chem. C* **2011**, *115*, 25535.
(41) Hummelshoj, J. S.; Blomqvist, J.; Datta, S.; Vegge, T.; Rossmeisl, J.; Thygesen, K. S.; Luntz, A. C.; Jacobsen, K. W.; Norskov, J. K. *J. Chem. Phys.* **2010**, 132.
(42) Albery, W. J.; Clark, D.; Drummond, H. J. J.; Coombs, A. J. M.; Young, W. K.; Hahn, C. E. W. *J. Electroanal. Chem.* **1992**, *340*, 99.
(43) Lu, Y.-C.; Kwabi, D. G.; Yao, K. P. C.; Harding, J. R.; Zhou, J.; Zuin, L.; Shao-Horn, Y. *Energy Environ. Sci.* **2011**, *4*, 2999.
(44) McCloskey, B. D.; Speidel, A.; Scheffler, R.; Miller, D. C.; Viswanathan, V.; Hummelshøj, J. S.; Nørskov, J. K.; Luntz, A. C. *J. Phys. Chem. Lett.* **2012**, 997.
(45) Jung, H.-G.; Hassoun, J.; Park, J.-B.; Sun, Y.-K.; Scrosati, B. *Nat. Chem.* **2012**, *4*, 579.
(46) Zhang, T.; Zhou, H. *Angew. Chem.* **2012**, *51*, 11062.
(47) Morita, M.; Goto, M.; Matsuda, Y. *J. Appl. Electrochem.* **1992**, *22*, 901.
(48) Anouti, M.; Dougassa, Y. R.; Tessier, C.; El Ouatani, L.; Jacquemin, J. *J. Chem. Thermodyn.* **2012**, *50*, 71.
(49) Peng, Z. Q.; Freunberger, S. A.; Chen, Y. H.; Bruce, P. G. *Science* **2012**, 337−563.
(50) Ottakam Thotiyl, M. M.; Freunberger, S. A.; Peng, Z.; Bruce, P. G. *J. Am. Chem. Soc.* **2012**, 135−494.